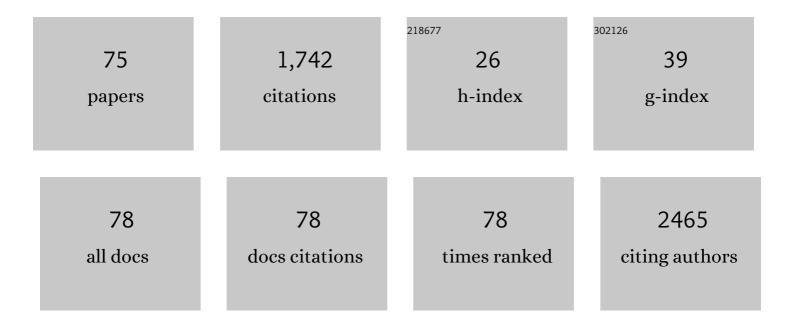
Matthias Stefan May

List of Publications by Year in descending order

Source: https://exaly.com/author-pdf/3612264/publications.pdf Version: 2024-02-01



#	Article	IF	CITATIONS
1	High-Pitch Spiral Computed Tomography. Investigative Radiology, 2011, 46, 116-123.	6.2	145
2	Dose Reduction in Abdominal Computed Tomography. Investigative Radiology, 2011, 46, 465-470.	6.2	119
3	Dual source multidetector CT-angiography before Transcatheter Aortic Valve Implantation (TAVI) using a high-pitch spiral acquisition mode. European Radiology, 2012, 22, 51-58.	4.5	101
4	Normalized Metal Artifact Reduction in Head and Neck Computed Tomography. Investigative Radiology, 2012, 47, 415-421.	6.2	66
5	Accuracy of prospectively ECG-triggered very low-dose coronary dual-source CT angiography using iterative reconstruction for the detection of coronary artery stenosis: comparison with invasive catheterization. European Heart Journal Cardiovascular Imaging, 2014, 15, 1238-1245.	1.2	65
6	Mammographic density as a risk factor for breast cancer in a German case–control study. European Journal of Cancer Prevention, 2011, 20, 1-8.	1.3	53
7	Low-Dose Dual-Source CT Angiography With Iterative Reconstruction for Coronary Artery Stent Evaluation. JACC: Cardiovascular Imaging, 2013, 6, 458-465.	5.3	50
8	Imaging the Parasinus Region with a Third-Generation Dual-Source CT and the Effect of Tin Filtration on Image Quality and Radiation Dose. American Journal of Neuroradiology, 2015, 36, 1225-1230.	2.4	49
9	Attenuation-Based Automatic Kilovolt Selection in Abdominal Computed Tomography. Investigative Radiology, 2012, 47, 559-565.	6.2	48
10	Low-Dose CT of the Paranasal Sinuses: Minimizing X-Ray Exposure with Spectral Shaping. European Radiology, 2016, 26, 4155-4161.	4.5	48
11	Induction and repair of DNA double-strand breaks in blood lymphocytes of patients undergoing 18F-FDG PET/CT examinations. European Journal of Nuclear Medicine and Molecular Imaging, 2012, 39, 1712-1719.	6.4	46
12	CT-based analysis of pericoronary adipose tissue density: Relation to cardiovascular risk factors and epicardial adipose tissue volume. Journal of Cardiovascular Computed Tomography, 2016, 10, 52-60.	1.3	45
13	Automatic detection of lytic and blastic thoracolumbar spine metastases on computed tomography. European Radiology, 2013, 23, 1862-1870.	4.5	42
14	Automated Tube Voltage Selection in Thoracoabdominal Computed Tomography at High Pitch Using a Third-Generation Dual-Source Scanner. Investigative Radiology, 2015, 50, 352-360.	6.2	42
15	Improved Image Quality in Head and Neck CT Using a 3D Iterative Approach to Reduce Metal Artifact. American Journal of Neuroradiology, 2015, 36, 1988-1993.	2.4	39
16	Frequency split metal artefact reduction in pelvic computed tomography. European Radiology, 2013, 23, 2137-2145.	4.5	37
17	Influence of Cardiac MR Imaging on DNA Double-Strand Breaks in Human Blood Lymphocytes. Radiology, 2015, 277, 406-412.	7.3	37
18	Radiation dose reduction in parasinus CT by spectral shaping. Neuroradiology, 2017, 59, 169-176.	2.2	36

10 Acute adverse events in cardiac MR imaging with gadolinium-based contrast agents: results from the European Society of Cardiovascular Radiology (ESCR) MRCT Registry in 72,839 patients. European Radiology, 2019, 29, 3868-3695. 4.5 ac 20 Dual-Energy Computed Tomography Angiography of the Head and Neck With Single-Source Computed Tomography. Investigative Radiology, 2016, 51, 618-623. 6.2 33 21 Influence of Different Antioxidants on X.Ray Induced DNA Double-Strand Breaks (DSBs) Using 1P-H2AX 2.5 32 22 Carotid CTA: Radiation Exposure and Image Quality with the Use of Attenuation-Based, Automated Klovolt Selection. American Journal of Neuroradiology, 2014, 35, 237-241. 2.4 31 23 Comparison of dual- and single-source dual-energy CT in head and neck Imaging. European Radiology, 2019, 29, 4207-4214. 2.0 26 24 Local Control of Perivascular Malignant Liver Lesions Using Percutaneous Inteversible Electroporation: Initial Experiences. CardioVascular and Interventional Radiology, 2015, 38, 152-159. 2.0 26 25 High-Pitch Thoracic CT With Simultaneous Assessment of Coronary Atteries. JACC: Cardiovascular Imaging, 2011, 4, 602-609. 2.2 26 26 Automated tube voltage adaptation in head and neck computed tomography between 120 and 100ÅkV: effects on image quality and radiation dose. Neuroradiology, 2014, 55, 797-803. 2.2 26 27 Epfect of Contrast-Enhance, 2020, 22,	TATIONS
20 Tomography. Investigative Radiology, 2016, 51, 618-623. 6.2 6.2 6.2 6.2 21 Influence of Different Antioxidants on X-Ray Induced DNA Double-Strand Breaks (DSBs) Using ¹² H2AX 2.5 53 22 Carotid CTA: Radiation Exposure and Image Quality with the Use of Attenuation-Based, Automated 2.4 31 23 Comparison of dual- and single-source dual-energy CT in head and neck Imaging. European Radiology, 2019, 29, 4207-4214. 4.5 31 24 Local Control of Perivascular Malignant Liver Lesions Using Percutaneous Inteversible 2.0 25 25 High-Pitch Thoracic CT With Simultaneous Assessment of Coronary Arteries. JACC: Cardiovascular 5.3 26 26 Automated tube voltage adaptation in head and neck computed tomography between 120 and 100ÅkV: 2.2 26 26 Automated tube voltage adaptation in head and neck computed tomography between 120 and 100ÅkV: 2.2 26 26 Automated Tube notic and Sports Physical Therapy. 2018, 48, 87-894. 3.5 26 27 Effect of Compression Carments on the Development of Delayed-Onset Muscle Soreness: A Multimodal Approach Using Cortrast Enhanced Ultrasound and Acoustic Radiation Force Impulse Elastography. Jourland of Cardiovascular Magnetic Resonance, 2020, 22, 39. 3.3 26 28 Cardi	
21 Immunofluorescence Microscopy in a Preliminary Study. PLoS ONE, 2015, 10, e0127142. 2.3 22 22 Carotid CTA: Radiation Exposure and Image Quality with the Use of Attenuation-Based, Automated Kilovok Selection. American Journal of Neuroradiology, 2014, 35, 237-241. 2.4 31 23 Comparison of dual- and single-source dual-energy CT in head and neck imaging. European Radiology, 2019, 29, 4207-4214. 4.5 31 24 Local Control of Perivascular Malignant Liver Lesions Using Percutaneous Irreversible Electroporation: initial Experiences. CardioVascular and Interventional Radiology, 2015, 38, 152-159. 2.0 26 25 High-Pitch Thoracic CT With Simultaneous Assessment of Coronary Arteries. JACC: Cardiovascular Imaging, 2011, 4, 602-609. 5.3 28 26 Automated tube voltage adaptation in head and neck computed tomography between 120 and 100ÅkV: effects on image quality and radiation dose. Neuroradiology, 2014, 56, 797-803. 2.2 26 27 Approach Using Contrast-Enhanced Ultrasound and Acoustic Radiation Force Impulse Elastography. Journal of Orthopaedic and Sports Physical Therapy, 2018, 48, 887-894. 3.3 26 28 Cardiac T2 mapping: robustness and homogeneity of standardized in-line analysis. Journal of Cardiovascular Magnetic Resonance, 2020, 22, 39. 3.3 26 29 Computed Tomography of the Head and Neck Region for Tumor StagingãeC"Comparison of Dual-Source, Dual-Energy and Low-Kilo	1
22 Kilovolt Selection. American Journal of Neuroradiology, 2014, 35, 237-241. 2.4 31 23 Comparison of dual- and single-source dual-energy CT in head and neck imaging. European Radiology, 2019, 29, 4207-4214. 4.5 31 24 Local Control of Perivascular Malignant Liver Lesions Using Percutaneous Irreversible Electroporation: Initial Experiences. CardioVascular and Interventional Radiology, 2015, 38, 152-159. 2.0 25 25 High-Pitch Thoracic CT With Simultaneous Assessment of Coronary Arteries. JACC: Cardiovascular funging, 2011, 4, 602-609. 5.3 26 26 Automated tube voltage adaptation in head and neck computed tomography between 120 and 100ÅkV: effects on image quality and radiation dose. Neuroradiology, 2014, 56, 797-803. 2.2 26 27 Effect of Compression Garments on the Development of Delayed-Onset Muscle Soreness: A Multimodal Approach Using Contrast-Enhanced Ultrasound and Accoustic Radiation Force Impulse Elastography. Journal of Orthopaedic and Sports Physical Therapy, 2018, 48, 87-894. 3.3 26 28 Cardiac T2 mapping: robustness and homogeneity of standardized in-line analysis. Journal of Cardiovascular Magnetic Resonance, 2020, 22, 39. 3.3 25 29 Computed Tomography of the Head and Neck Region for Tumor Stagingåé"Comparison of Dual-Source, Dual-Energy and Low-Kilovolt, Single-Energy Acquisitions. Investigative Radiology, 2017, 52, 522-528. 6.2 22 30 Quan	
2019, 29, 42074214. 4.0 4.0 5.0 24 Local Control of Perivascular Malignant Liver Lesions Using Percutaneous Irreversible Electroporation: Initial Experiences. CardioVascular and Interventional Radiology, 2015, 38, 152-159. 2.0 25 25 High-Pitch Thoracic CT With Simultaneous Assessment of Coronary Arteries. JACC: Cardiovascular 5.3 28 26 Automated tube voltage adaptation in head and neck computed tomography between 120 and 100ÅkV: effects on image quality and radiation dose. Neuroradiology, 2014, 56, 797-803. 2.2 26 27 Approach Using Contrast-Enhanced Ultrasound and Acoustic Radiation Force Impulse Elastography. Journal of Orthopaedic and Sports Physical Therapy, 2018, 48, 887-894. 3.5 26 28 Cardiac T2 mapping: robustness and homogeneity of standardized in-line analysis. Journal of Cardiovascular Magnetic Resonance, 2020, 22, 39. 3.3 25 29 Computed Tomography of the Head and Neck Region for Tumor Stagingâ€"Comparison of Dual-Source, Dual-Energy and Low-Kilovolt, Single-Energy Acquisitions. Investigative Radiology, 2017, 52, 522-528. 6.2 22 30 Quantitative T2 Mapping Shows Increased Degeneration in Adjacent Intervertebral Discs Following Kyphoplasty. Cartilage, 2020, 11, 152-159. Myocardial Adaptation to High-Intensity (Interval) Training in Previously Untrained Men With a Longitudinal Cardiovascular Magnetic Resonance Imaging Study (Running Study and Heart Tria). 2.6 19 </td <td></td>	
24 Electroporation: Initial Experiences. CardioVascular and Interventional Radiology, 2015, 38, 152-159. 2.0 25 25 High-Pitch Thoracic CT With Simultaneous Assessment of Coronary Arteries. JACC: Cardiovascular 5.3 26 26 Automated tube voltage adaptation in head and neck computed tomography between 120 and 100ÅkV: 2.2 26 27 Automated tube voltage adaptation dose. Neuroradiology, 2014, 56, 797-803. 2.2 26 27 Effect of Compression Garments on the Development of Delayed-Onset Muscle Soreness: A Multimodal 3.5 26 28 Cardiac T2 mapping: robustness and homogeneity of standardized in-line analysis. Journal of Orthopaedic and Sports Physical Therapy, 2018, 48, 887-894. 3.3 26 29 Computed Tomography of the Head and Neck Region for Tumor Stagingâ€"Comparison of Dual-Source, Dual-Energy and Low-Kilovolt, Single-Energy Acquisitions. Investigative Radiology, 2017, 52, 522-528. 6.2 22 30 Quantitative T2 Mapping Shows Increased Degeneration in Adjacent Intervertebral Discs Following Kyphoplasty. Cartilage, 2020, 11, 152-159. 2.7 22 31 Longitudinal Cardiovascular Magnetic Resonance Imaging Study (Running Study and Heart Trial). 2.6 19	
25 Imaging, 2011, 4, 602-609. 5.3 28 26 Automated tube voltage adaptation in head and neck computed tomography between 120 and 100ÅkV: effects on image quality and radiation dose. Neuroradiology, 2014, 56, 797-803. 2.2 26 27 Effect of Compression Garments on the Development of Delayed-Onset Muscle Soreness: A Multimodal Approach Using Contrast-Enhanced Ultrasound and Acoustic Radiation Force Impulse Elastography. Journal of Orthopaedic and Sports Physical Therapy, 2018, 48, 887-894. 3.5 26 28 Cardiac T2 mapping: robustness and homogeneity of standardized in-line analysis. Journal of Cardiovascular Magnetic Resonance, 2020, 22, 39. 3.3 26 29 Computed Tomography of the Head and Neck Region for Tumor Stagingãé"Comparison of Dual-Source, Dual-Energy and Low-Kilovolt, Single-Energy Acquisitions. Investigative Radiology, 2017, 52, 522-528. 6.2 22 30 Quantitative T2 Mapping Shows Increased Degeneration in Adjacent Intervertebral Discs Following Kyphoplasty. Cartilage, 2020, 11, 152-159. 2.7 22 31 Myocardial Adaptation to High-Intensity (Interval) Training in Previously Untrained Men With a Longitudinal Cardiovascular Magnetic Resonance Imaging Study (Running Study and Heart Trial). 2.6 19)
26 effects on image quality and radiation dose. Neuroradiology, 2014, 56, 797-803. 2.2 26 27 Effect of Compression Garments on the Development of Delayed-Onset Muscle Soreness: A Multimodal 3.5 26 27 Approach Using Contrast-Enhanced Ultrasound and Acoustic Radiation Force Impulse Elastography. 3.5 26 28 Cardiac T2 mapping: robustness and homogeneity of standardized in-line analysis. Journal of 3.3 25 29 Computed Tomography of the Head and Neck Region for Tumor Stagingâ€"Comparison of Dual-Source, Dual-Energy and Low-Kilovolt, Single-Energy Acquisitions. Investigative Radiology, 2017, 52, 522-528. 6.2 22 30 Quantitative T2 Mapping Shows Increased Degeneration in Adjacent Intervertebral Discs Following Kyphoplasty. Cartilage, 2020, 11, 152-159. 2.7 25 31 Longitudinal Cardiovascular Magnetic Resonance Imaging Study (Running Study and Heart Trial). 2.6 19	
 Approach Using Contrast-Enhanced Ultrasound and Acoustic Radiation Force Impulse Elastography. Journal of Orthopaedic and Sports Physical Therapy, 2018, 48, 887-894. Cardiac T2 mapping: robustness and homogeneity of standardized in-line analysis. Journal of Cardiovascular Magnetic Resonance, 2020, 22, 39. Computed Tomography of the Head and Neck Region for Tumor Stagingâ€"Comparison of Dual-Source, Dual-Energy and Low-Kilovolt, Single-Energy Acquisitions. Investigative Radiology, 2017, 52, 522-528. Quantitative T2 Mapping Shows Increased Degeneration in Adjacent Intervertebral Discs Following Quantitation to High-Intensity (Interval) Training in Previously Untrained Men With a Longitudinal Cardiovascular Magnetic Resonance Imaging Study (Running Study and Heart Trial). 	
28 Cardiovascular Magnetic Resonance, 2020, 22, 39. 3.3 26 29 Computed Tomography of the Head and Neck Region for Tumor Stagingâ€"Comparison of Dual-Source, Dual-Energy and Low-Kilovolt, Single-Energy Acquisitions. Investigative Radiology, 2017, 52, 522-528. 6.2 22 30 Quantitative T2 Mapping Shows Increased Degeneration in Adjacent Intervertebral Discs Following Kyphoplasty. Cartilage, 2020, 11, 152-159. 2.7 22 31 Myocardial Adaptation to High-Intensity (Interval) Training in Previously Untrained Men With a Longitudinal Cardiovascular Magnetic Resonance Imaging Study (Running Study and Heart Trial). 2.6 19	
29 Dual-Energy and Low-Kilovolt, Single-Energy Acquisitions. Investigative Radiology, 2017, 52, 522-528. 6.2 22 30 Quantitative T2 Mapping Shows Increased Degeneration in Adjacent Intervertebral Discs Following Kyphoplasty. Cartilage, 2020, 11, 152-159. 2.7 22 31 Myocardial Adaptation to High-Intensity (Interval) Training in Previously Untrained Men With a Longitudinal Cardiovascular Magnetic Resonance Imaging Study (Running Study and Heart Trial). 2.6 19	i
S0 Kyphoplasty. Cartilage, 2020, 11, 152-159. 2.7 22 Myocardial Adaptation to High-Intensity (Interval) Training in Previously Untrained Men With a 31 Longitudinal Cardiovascular Magnetic Resonance Imaging Study (Running Study and Heart Trial). 2.6 19	
31 Longitudinal Cardiovascular Magnetic Resonance Imaging Study (Running Study and Heart Trial). 2.6 19	<u>'</u>
Computed Tomography Angiography of Carotid Arteries and Vertebrobasilar System. Medicine (United) Tj ETQq0 0.0 rgBT /Oye	rlock 10
A Novel Pairwise Comparison-Based Method to Determine Radiation Dose Reduction Potentials of 33 Iterative Reconstruction Algorithms, Exemplified Through Circle of Willis Computed Tomography 6.2 18 Angiography. Investigative Radiology, 2016, 51, 331-339.	
34Stent evaluation in low-dose coronary CT angiography: Effect of different iterative reconstruction1.31734settings. Journal of Cardiovascular Computed Tomography, 2013, 7, 319-325.1.317	
Diagnostic Accuracy of an MRI Protocol of the Knee Accelerated Through Parallel Imaging in 35 Correlation to Arthroscopy. RoFo Fortschritte Auf Dem Gebiet Der Rontgenstrahlen Und Der 1.3 17 Bildgebenden Verfahren, 2018, 190, 265-272.	

³⁶³D Dixon water-fat LGE imaging with image navigator and compressed sensing in cardiac MRI. European
Radiology, 2021, 31, 3951-3961.4.517

MATTHIAS STEFAN MAY

#	Article	IF	CITATIONS
37	Effect of Compression Garments on the Development of Edema and Soreness in Delayed-Onset Muscle Soreness (DOMS). Journal of Sports Science and Medicine, 2018, 17, 392-401.	1.6	16
38	Glucocorticoid-induced relapse of COVID-19 in a patient with sarcoidosis. Annals of the Rheumatic Diseases, 2021, 80, e87-e87.	0.9	15
39	Individual Calculation of Effective Dose and Risk of Malignancy Based on Monte Carlo Simulations after Whole Body Computed Tomography. Scientific Reports, 2020, 10, 9475.	3.3	14
40	Preoperative assessment of the aortic arch in children younger than 1 year with congenital heart disease: utility of low-dose high-pitch dual-source computed tomography. A single-centre, retrospective analysis of 62 cases. European Journal of Cardio-thoracic Surgery, 2014, 45, 1060-1065.	1.4	13
41	Contrast medium application in pediatric high-pitch cardiovascular CT angiography: Manual or power injection?. Journal of Cardiovascular Computed Tomography, 2014, 8, 315-322.	1.3	11
42	Evaluation of ventricular septal defects using high pitch computed tomography angiography of the chest in children with complex congenital heart defects below one year of age. Journal of Cardiovascular Computed Tomography, 2019, 13, 226-233.	1.3	9
43	Comparison of Readout-Segmented Echo-Planar Imaging and Single-Shot TSE DWI for Cholesteatoma Diagnostics. American Journal of Neuroradiology, 2021, 42, 1305-1312.	2.4	9
44	Improving the Safety of DIEP Flap Transplantation: Detailed Perforator Anatomy Study Using Preoperative CTA. Journal of Personalized Medicine, 2022, 12, 701.	2.5	9
45	Radiation dose considerations by intra-individual Monte Carlo simulations in dual source spiral coronary computed tomography angiography with electrocardiogram-triggered tube current modulation and adaptive pitch. European Radiology, 2012, 22, 569-578.	4.5	8
46	Cone Beam CT Imaging of the Paranasal Region with a Multipurpose X-ray System—Image Quality and Radiation Exposure. Applied Sciences (Switzerland), 2020, 10, 5876.	2.5	8
47	Achieving high spatial and temporal resolution with perfusion MRI in the head and neck region using golden-angle radial sampling. European Radiology, 2021, 31, 2263-2271.	4.5	8
48	Personalized Chest Computed Tomography. Investigative Radiology, 2022, 57, 148-156.	6.2	8
49	Image quality, diagnostic accuracy, and potential for radiation dose reduction in thoracoabdominal CT, using Sinogram Affirmed Iterative Reconstruction (SAFIRE) technique in a longitudinal study. PLoS ONE, 2017, 12, e0180302.	2.5	8
50	Whole body magnetic resonance angiography and computed tomography angiography in the vascular mapping of head and neck: an intraindividual comparison. Head & Face Medicine, 2014, 10, 16.	2.1	7
51	Feasibility of Respiratory-gated High-pitch Spiral CT:. Academic Radiology, 2016, 23, 406-412.	2.5	7
52	Single source split filter dual energy: Image quality and liver lesion detection in abdominal CT. European Journal of Radiology, 2020, 126, 108913.	2.6	5
53	Myocardial adaption to HI(R)T in previously untrained men with a randomized, longitudinal cardiac MR imaging study (Physical adaptions in Untrained on Strength and Heart trial, PUSH-trial). PLoS ONE, 2017, 12, e0189204.	2.5	5
54	Native cardiac T1 Mapping: Standardized inline analysis of long and short axis at three identical 1.5 Tesla MRI scanners. European Journal of Radiology, 2018, 107, 203-208.	2.6	4

#	Article	IF	CITATIONS
55	Complete Free-breathing Adenosine Stress Cardiac MRI Using Compressed Sensing and Motion Correction: Comparison of Functional Parameters, Perfusion, and Late Enhancement with the Standard Breath-holding Examination. Radiology: Cardiothoracic Imaging, 2019, 1, e180017.	2.5	4
56	Cardiac T2 star mapping: standardized inline analysis of long and short axis at three identical 1.5ÂT MRI scanners. International Journal of Cardiovascular Imaging, 2019, 35, 695-702.	1.5	4
57	Dual-source computed tomography of the lung with spectral shaping and advanced iterative reconstruction: potential for maximum radiation dose reduction. Pediatric Radiology, 2020, 50, 1240-1248.	2.0	4
58	Which concentration to choose in dual flow cardiac CT?. European Journal of Radiology, 2012, 81, e461-e466.	2.6	3
59	Extent of simultaneous radiation dose and iodine reduction at stable image quality in computed tomography of the chest. Medicine (United States), 2018, 97, e0388.	1.0	3
60	Carotid CTA at the Lowest Tube Voltage (70 kV) in Comparison with Automated Tube Voltage Adaption. American Journal of Neuroradiology, 2019, 40, 1374-1382.	2.4	3
61	Mobile Workflow in Computed Tomography of the Chest. Journal of Medical Systems, 2019, 43, 14.	3.6	3
62	Pilot study using intraoperative fluorescence angiography during arteriovenous hemodialysis access surgery. Journal of Vascular Access, 2019, 20, 175-183.	0.9	3
63	Organ-specific context-sensitive CT image reconstruction and display. , 2018, , .		3
64	The third dimension in perforator mapping—Comparison of Cinematic Rendering and maximum intensity projection in abdominal-based autologous breast reconstruction. Journal of Plastic, Reconstructive and Aesthetic Surgery, 2022, 75, 536-543.	1.0	3
65	Dual-Energy Lung Perfusion in Portal Venous Phase CT—A Comparison with the Pulmonary Arterial Phase. Diagnostics, 2021, 11, 1989.	2.6	3
66	Influence of risk-organ–based tube current modulation on CT-induced DNA double-strand breaks in a biological phantom model. Journal of Radiation Research, 2018, 59, 692-699.	1.6	2
67	Effect of long term CPAP therapy on cardiac parameters assessed with cardiac MRI. International Journal of Cardiovascular Imaging, 2021, 37, 613-621.	1.5	2
68	Potential for Radiation Dose Reduction in Dual-Source Computed Tomography of the Lung in the Pediatric and Adolescent Population Compared to Digital Radiography. Diagnostics, 2021, 11, 270.	2.6	2
69	Evaluation of CT-Guided Ultra-Low-Dose Protocol for Injection Guidance in Preparation of MR-Arthrography of the Shoulder and Hip Joints in Comparison to Conventional and Low-Dose Protocols. Diagnostics, 2021, 11, 1835.	2.6	2
70	Determining Microvascular Obstruction and Infarct Size with Steady-State Free Precession Imaging Cardiac MRI. PLoS ONE, 2015, 10, e0119788.	2.5	2
71	Image quality comparison of single-energy and dual-energy computed tomography for head and neck patients: a prospective randomized study. European Radiology, 2022, 32, 7700-7709.	4.5	2
72	Cutting Staff Radiation Exposure and Improving Freedom of Motion during CT Interventions: Comparison of a Novel Workflow Utilizing a Radiation Protection Cabin versus Two Conventional Workflows. Diagnostics, 2021, 11, 1099.	2.6	1

#	Article	IF	CITATIONS
73	Prognostic Value of CTA-Derived Left Ventricular Mass in Neonates with Congenital Heart Disease. Diagnostics, 2021, 11, 1215.	2.6	1
74	Dynamic CT angiography for therapy evaluation after transarterial chemoembolization of hepatocellular carcinoma. Acta Radiologica, 2020, 61, 148-155.	1.1	0
75	Cor Triatriatum Sinistrum Combined with Changes in Atrial Septum and Right Atrium in a 60-Year-Old Woman. Medicina (Lithuania), 2021, 57, 777.	2.0	0